Unified Global and Regional Wave Model on a Multi-Resolution Grid

JIAN-GUO LI* AND ANDREW SAULTER
Met Office, Exeter EX1 3PB, United Kingdom

1. Introduction

Models for ocean surface wave forecasting in weather centres comprise global and regional systems in order to efficiently meet service demands. Most regional models aim to resolve details near coastlines and be compatible with high resolution atmospheric models. However, these regional models cannot run alone and have to use large area or global models to provide boundary wave spectra. The most traditional nesting technique is actually running the two models together with the regional model domain covered by both resolutions. Two way schemes have also been developed, but still require an overlapping 'stencil area'. Using an unstructured grid technique, this overlapping may be avoided and boundary conditions can be simplified by flexible positioning of boundaries.

A spherical multiple-cell (SMC) grid (Li 2011) is designed to relax the CFL restriction of Eulerian advection time step at high latitudes by merging the conventional lat-lon grid cells as in the reduced grid (Rasch 1994). It solves the polar problem by introducing a polar cell and fixing the wave spectral reference direction within a high latitude circle. These polar features of the SMC grid allow wave models to be extended to high latitudes or even the whole Arctic if the Arctic sea-ice disappears in future summers. The unstructured feature of the SMC grid allows land cells to be removed from of the model and boundaries to fit irregular coastlines.

A particular feature of the SMC grid is that it supports refined resolutions with reduced sub-time steps, leading to an efficient multi-resolution grid. The SMC grid has been implemented in the latest version of the WAVEWATCH III (Tolman 1991, Tolman et al. 2002). Additional efficiencies have been incorporated into wave propagation schemes, including an upstream non-oscillatory 2nd-order (UNO2) advection scheme (Li 2008), which saves about 30% advection time in comparison with the original 3rd-order scheme, and a rotational refraction scheme, which removes the refraction angle limit imposed by the original advection alike refraction scheme (Li 2012). This SMC grid is used here to merge high resolution regional models into a coarse resolution global model so that a single unified model could be used to replace the multi-model operational forecasting suite.

The SMC grid can also be used for regional models like other unstructured grids. It would be particularly useful for applications in irregular areas, such as the Great Lakes, the Mediterranean Sea and even the whole Atlantic. The former two regions do not need any boundary conditions (if the Strait of Gibraltar is negligible) and can be run as independent models. Even for the Atlantic model, the unstructured grid allows the model domain to be extended conveniently to minimise boundary conditions. Results from these 3 regional models will also be demonstrated. In comparison with the existing unstructured finite element grid in the WAVEWATCH III model (Roland et al 2009), the SMC grid retains the finite difference schemes on the conventional lat-lon meshes. Hence the SMC grid is simpler and faster than the finite element grid.

Besides, unresolved small islands incur errors in global ocean surface wave models as they are important sinks of the ocean surface wave energy (Tolman 2003). Missed island groups in coarse resolution global models lead to a persistent under-prediction of wave energy blocking. Although the far field errors can be alleviated with sub-grid obstructions, high resolution around islands is still the most appropriate approach for accurate swell prediction close to islands (Chawla and Tolman 2008). The unstructured SMC grid can resolve small islands and coastlines with refined resolutions while

* *Corresponding author address*: Dr Jian-Guo Li, Met Office, FitzRoy Road, Exeter EX1 3PB, UK
Email: Jian-Guo.Li@metoffice.gov.uk *Tel.* +44 1392 884885 *Fax.* +44 1392 885681

keeping the vast open oceans at an affordable resolution. This is an additional advantage of this unified model.

This paper outlines the essential formulation of the SMC grid and illustrates its features with a unified mode at 25 km global resolution and refined 12 km and 6 km resolutions near coastlines and in the European region. The 3-tiered (6-12-15 km) global multi-resolution SMC grid (SMC6125) has been validated with buoy data and compared with a 25 km global lat-lon (G25) model. Here the SMC6125 grid is compared with the Met Office operational global 30km (G30) grid, European 8 km (Euro8) and UK 4km (UK4) regional grids. Other examples of the SMC grid for the Atlantic Ocean and the Great Lakes are also demonstrated.

2. Wave propagation on a sphere

The Eulerian ocean surface wave model is based on a 2D spectral energy balance equation. In the 2-D spherical coordinates with longitude λ and latitude φ, the equation is given by

$$\begin{aligned}
&\frac{\partial \psi}{\partial t}+\frac{\partial F_x}{\partial x}+\frac{\partial (F_y \cos\varphi)}{\cos\varphi \partial y}+\frac{\partial (\dot{k}\psi)}{\partial k}+\frac{\partial (\dot{\theta}\psi)}{\partial \theta}=S \\
&F_x \equiv u\psi - D_x \partial\psi/\partial x \\
&F_y \equiv \upsilon\psi - D_y \partial\psi/\partial y
\end{aligned} \tag{1}$$

where $\psi(t, \lambda, \varphi, k, \theta)$ is any component of the wave energy spectrum, t is the time, k is the wave number, θ is the spectral direction usually defined from the local east direction, u and υ are the zonal and meridian components of the wave energy propagation speed, D_x and D_y are the diffusion coefficients, and S the source term. The geophysical coordinates x and y are defined locally eastward along the parallel and northward along the meridian, respectively. Their increments are given by $dx = r\cos\varphi d\lambda$, $dy = rd\varphi$, where r is the radius of the sphere. The overhead dot indicates time differentiation along the wave propagation path. The r.h.s S represents all source terms and they are unchanged from the original WW3 model. Note that in WW3 model the wave action $A \equiv \psi/\omega$, where ω is the intrinsic angular frequency of the ocean surface wave, is chosen instead of the wave energy ψ for conservation when ocean current is present. The wave action shares the same equation (1) as the wave energy except that the source term is divided by ω. Hence all propagation schemes for wave energy can be applied on wave action.

The spherical wave energy balance equation (1) differs from its Cartesian counterpart in the meridian differential term by an extra cosine factor, which renders the term undefined (singular) at the Poles. Thus, except for at the Poles, Eq. (1) can be approximated with finite-difference schemes similar to those used in the Cartesian grid. The only difference between the Cartesian and spherical versions of these finite-difference schemes is that the latter has an extra cosine factor. Because the SMC grid retains the lat-lon grid cells, the wave energy balance equation (1) is also valid on the SMC grid.

The diffusion term in (1) may be considered as the sub-grid mixing term because the model wave spectrum represents the spatial average over one grid cell. This diffusion term is usually parameterised to alleviate the so called garden-sprinkler effect (GSE) due to discretization of the wave energy spectrum (Booij and Holthuijsen 1987, Tolman 2002).

One primary physical process that affects surface wave propagation is the depth-induced refraction. Refraction formulations in contemporary surface wave models are based on the linear wave theory, assuming slow-varying ocean depth. The refraction on the SMC grid follows the same formulations in the WW3 (Tolman 1991):

$$\dot{k} = -\xi \mathbf{k} \cdot \nabla h - \mathbf{k} \cdot \nabla U_k \tag{2a}$$

$$\dot{\theta}_{rfr} = -\xi \mathbf{n} \cdot \nabla h - \mathbf{n} \cdot \nabla U_k \tag{2b}$$

where **k** =($k\cos\theta$, $k\sin\theta$) is the wave number vector, h is the water depth, ∇ is the 2-D gradient operator, U_k is the ambient current velocity component along the **k** direction, $\xi = \omega / \sinh(2kh)$ will be referred to as the *refraction factor* and and **n** = ($-\sin\theta$, $\cos\theta$) is a unit vector normal to the **k** direction to the left or at $\theta + \pi/2$. The wave number change rate (2a) is also known as the spectral shift and the direction change rate (2b) is called the refraction rate. More details on derivation of these refraction rates are available in Li (2012).

Wave energy travels along the shortest route on the ocean surface, that is, along great circles on the sphere. So a wave spectral component will not be confined at its defined direction but will shift gradually with latitude along its great circle path, a procedure known as great circle turning (GCT). Assuming the great circle direction is at an angle θ from the local east direction at latitude φ, the product of cosines of these two angles is conserved on the great circle path, that is, $\cos\theta\cos\varphi = const.$, which provides a simple rule for navigation along great circles and leads to the following GCT rate along the propagation direction

$$\dot{\theta}_{gct} = -\left(c_g / r\right)\cos\theta\tan\varphi \tag{3}$$

where c_g is the wave group speed defined by

$$c_g = c_{gd}\left(\tanh(kh) + kh/\cosh^2(kh)\right) \tag{4}$$

in which $c_{gd} = g/2\omega$ is the group speed in deep waters. The net wave direction changing rate used in (1) for the SMC grid is then the sum of the refraction rate (2b) and the GCT rate (3).

3. Numerical schemes on a SMC grid

Scalar advection schemes on the SMC grid are described in Li (2011). Here summarised are other terms in (1) and treatment of advection and diffusion on the multi-resolution SMC grid. It also tackles the polar problem with vector components at high latitudes.

3.1. SMC grid cell and face arrays

A global SMC grid is shown in Fig.1. For clarity, only the Arctic region is shown here. The highest resolution of the SMC grid (for size-1) cell is set to be $\Delta\lambda$ = 360º/(1024*4) = 0.3515625º/4 and $\Delta\varphi$ = 180º/(768*4) = 0.234375º/4 and the latitudinal grid length is about 6 km. The SMC grid uses only the sea points or cells and refines the resolution by two levels to 6 km around islands and coastlines, resulting in a global 3-level (6-12-25 km) SMC grid on ocean surface. This SMC grid will be referred to as the SMC6-25 grid. Cells are merged longitudinally at high latitudes following the same rules in Li (2011) to relax the CFL restriction. A unique 5-element integer array is assigned to each cell to hold its SW corner x-, y-indices (i, j), cell x-, y-sizes (Δi, Δj), and water depth (h), as illustrated in Fig.2. The x- and y-indices are measured in size-1 cell increment so the cell centre latitude and longitude can be worked out with

$$\varphi_j = (j_0 + j + 0.5 * \Delta j)\Delta\varphi; \qquad \lambda_i = (i_0 + i + 0.5 * \Delta i)\Delta\lambda \tag{5}$$

where i_0 and j_0 are the origin of the cell x- and y-indices relative to the zero-meridian and the Equator, respectively. For the SMC6-25 grid, the origin of the grid indices is set at zero-meridian on the Equator so both i_0 and j_0 are zero. The mapping rule (5) is exactly the same as that for the lat-lon grid cells except for that the SMC grid cells are not arranged in spatial sequence (hence is called an unstructured grid) and their sizes may change by a multiple of 2 (size-1, size-2, size-4, …). The depth h is also rounded to an integer so the whole cell array can be declared as an integer array. The cells are listed as a 1-D array and sorted by their y-size for use of sub-time steps on refined cells. Please note that the sorting is on the y-size not the x-size because the cell x-size may change on the same resolution level due to the longitudinal merging at high latitudes. The cell y-size will be in ascending order in the sorted cell array list and the number of cells for each resolution level (of a given *y*-size) is listed on the first line of the cell array file after the total cell number. This cell number counts will be used for declaring the cell array variable and setting up the sub-loops for propagation schemes.

It should be emphasized that the cell size has to be increased no more than 1 level for any neighbouring cells, that is, around a size-1 cell the neighbouring cells can be either size-1 or size-2. Similarly, size-2 cells can be linked to cells of the same size-2 or either 1-level down (size-1) or 1-level up (size-4). This 1-level size change rule ensures resolution varies gradually and simplifies the face flux formulation. Putting cells of more than 1 level difference in sizes sided by side would jeopardise the present face array generating program.

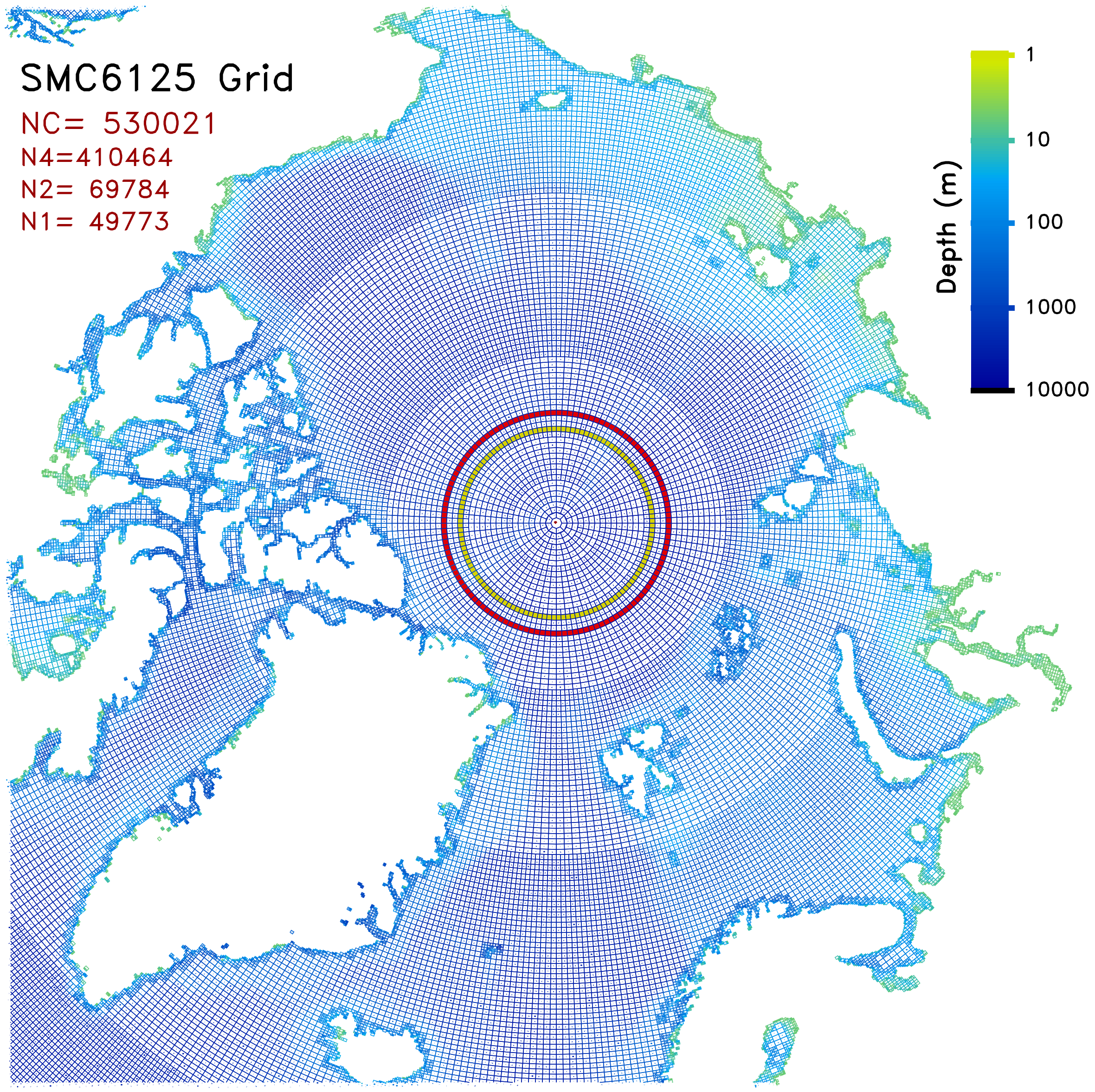

Fig.1. The Arctic part of the SMC6125 grid.

Once the cell arrays are compiled in the sorted order, cell face arrays can be generated with an extra FORTRAN code. Cell faces are named by its normal velocity components as *u*- or *υ*-faces. An 7-element integer array is pre-calculated for each face to store its face position, size, and its upstream-central-downstream (UCD) cell indices. An extra *y*-size integer is added for the υ-face array for sorting purposes. Face sizes are chosen to be the minimum size between the two neighbouring cells. For a cell face neighbouring two cells of 1-level below, the face is divided into two faces of the lowered level size. This minimised face size ensures one face links two cells only. The face arrays are also sorted by its *y*-size so that the multi-resolution advection/diffusion loops can be divided into multi-step sub-loops. The total face number and sub-level face numbers are listed on the first line of the face array file for propagation and mapping purposes. The face arrays are used to calculate the advection-diffusion and the depth gradient.

For the unified model, the SMC6-25 grid is refined in the Euro8 and UK4 regions at 12 km resolution by replacing size-4 cells with size-2 cells. This refined grid is referred to as the SMC6125 grid. Outside the Euro8 region, the SMC6125 grid is identical to the SMC6-25 grid so its global buoy comparison results are identical to those of the SMC6-25 grid shown in Li (2012).

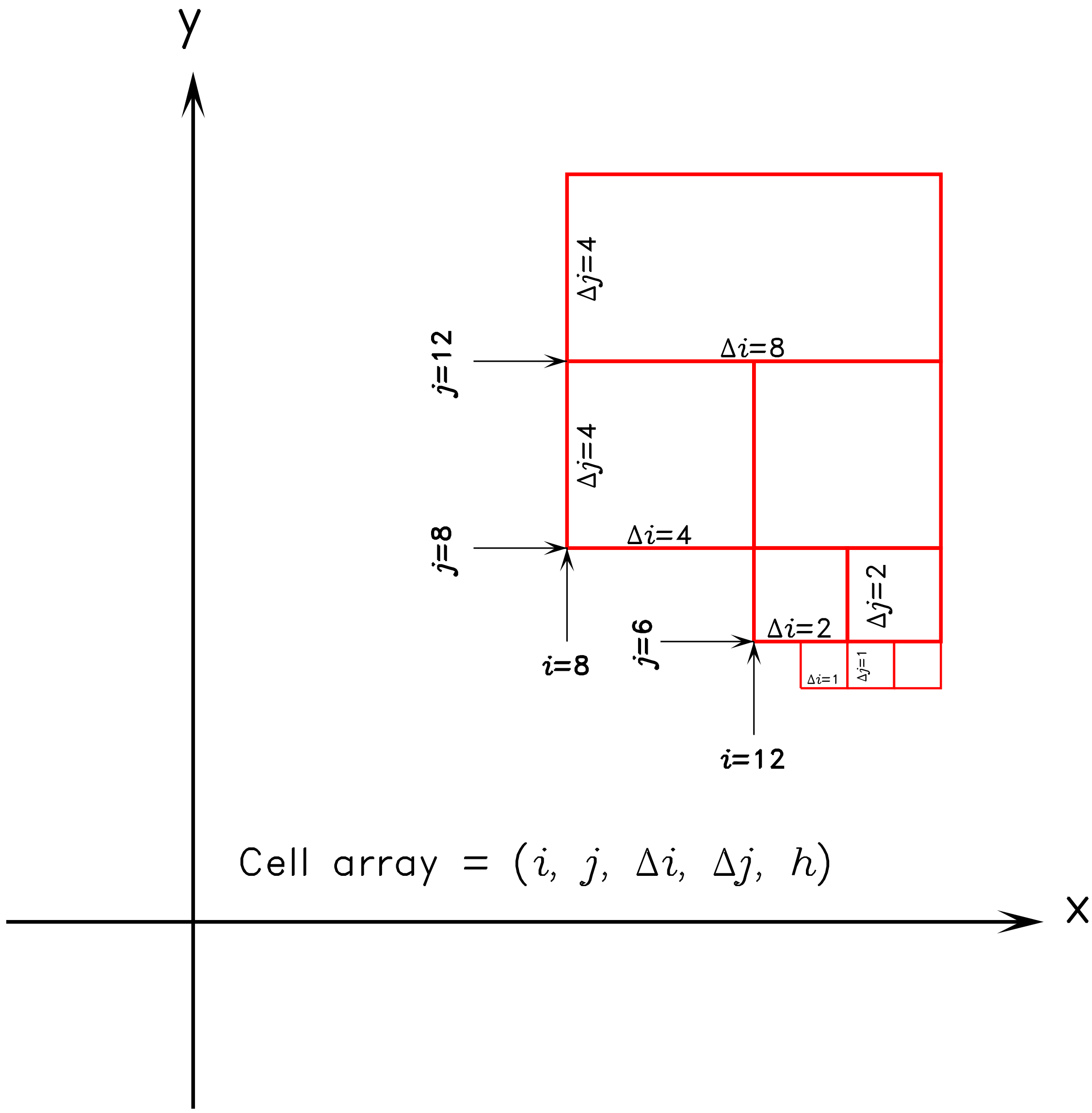

Fig.2. Illustration of SMC grid cell arrays.

3.2. Advection-diffusion schemes

The l.h.s terms in (1) are calculated with time-splitting approaches by combining the first (time differential) term with each of the other 4 terms. The advection-diffusion terms are discretised on the SMC grid with one flux loop and one cell loop for each dimension. Note that the diffusion term used here is slightly different from the original GSE smoothing term (Booij and Holthuijsen 1987). The original diffusion term is designed to enhance the transverse smoothing because a first order upstream advection scheme is used and it has already introduced strong smoothing along the wave propagation direction. The asymmetrical diffusion results in a cross term in Cartesian coordinates. In this SMC grid wave model, the advection is estimated with an upstream non-oscillatory 2nd order (UNO2) scheme (Li 2008), which is adapted from the MINMOD scheme (Roe 1985). As the implicit diffusion of the 2nd order advection scheme is much smaller than that of the first order scheme, the diffusion term is simplified to be isotropic so the cross-term vanishes. Besides, the refraction and GCT term provides extra directional smoothing, which makes the total smoothing biased towards the transverse direction, similar to the original asymmetrical smoothing term.

The advection flux with the UNO2 scheme and the diffusion flux with a central-space finite difference scheme for a u-face between the central and downstream cells are merged into a single flux, given by

$$\Delta F_x = \left(u\,\psi * - D_x G_{DC} \right) l_u \Delta t \tag{6}$$

where $\psi*$ is the mid-flux value evaluated with the UNO2 scheme (see Eq. (6) in Li 2008), $G_{DC} = (\psi_D - \psi_C)/(x_D - x_C)$ is the gradient between the central and downstream cells, l_u is the u-face length and Δt is the sub-time step. Both the advection and diffusion schemes are of 2nd order accuracy. In the presence of an ambient ocean current, the wave energy propagation speed in the x-direction should be the sum of the group speed and current speed components, that is, $u = c_g \cos\theta + U_x$.

The diffusion coefficient, $D_x = D_y$, is specified by the spectral component propagation speed, directional bin width and a user input swell age parameter as the transverse diffusion coefficient D_{nn} in the original model. The swell age has the same meaning as in the regular grid WW3 model and it has to be adjusted according to the base-level grid length and the advection time step (diffusion is calculated at the same time step as advection) to ensure the maximum Fourier number is less than 1 or usually set to be 0.5. A guide rule for the maximum swell age T_s is given by

$$D_x = \left(\frac{c_{gd}\Delta\theta}{\Delta x_0} \right)^2 \frac{\Delta t_a T_s}{12} \le \frac{1}{2}, \quad or \quad T_s \le \frac{6}{\Delta t_a} \left(\frac{\Delta x_0}{c_{gm}\Delta\theta} \right)^2 \tag{7}$$

in which Δt_a is the advection time step, Δx_0 is the base level grid length on the Equator, $\Delta\theta$ is the directional bin width (in radian) and c_{gm} is the maximum deep water group speed (c_{gd}) in the model spectral range (usually at the lowest frequency end). If the swell age is set too large, the diffusion term will become unstable and eventually bring the model to a crash. It would be convenient if the swell age was reduced automatically inside the model when users accidentally set it too large. This automatic adjustment, however, has not been set up yet.

A temporary net-flux variable, F_{net}, is used for each cell to gather all fluxes into the cell before it is used for the cell value update. The flux (6) is added to the downstream cell net-flux variable and subtracted from the central cell net-flux variable at the same time for energy conservation. The use of face sizes and the net flux variables allow fluxes from different sized faces to be added up in proportion to their face sizes. After the face loop is completed, each cell value is updated in a cell loop by

$$\psi^{n+1} = \psi^n + F_{net} / \left(l_x l_y \right) \tag{8}$$

where $l_{x/y}$ is the cell x/y-length. The cell y-length is required for x-flux update to cancel the face length used in sum of the fluxes in proportion to the u-face length. The υ-face fluxes are calculated similarly except for the additional latitude cosine factor.

For the multi-resolution SMC6-25 grid, the face and cell loops are sorted into 3 sub-loops according to their y-sizes, thanks to the unstructured nature of the SMC grid. Advection-diffusion terms for the refined 6- and 12-km cells are calculated at ¼ and ½ of the base level time step, that is, the 6-km flux and cell loops are done twice before the 12-km flux and cell loops are calculated once. The base level flux and cell loops are only calculated at each base level time step. The temporary net-flux variable is used to accumulate fluxes between different levels and is reset to zero once it is used for its cell update. The simple loop–regrouping technique for multi-resolution SMC grid allows a smooth transfer from a single resolution SMC grid to a multi-resolution grid with optimised efficiency.

Another feature of the SMC grid is the unification of boundary conditions with internal flux evaluations. Cell faces at coastlines are assumed to be bounded by two consecutive empty cells when the face arrays are generated. Thus, any wave energy transported into these empty cells will disappear, and no wave energy will be injected out of these zero cells into any sea cells. This convenient setup conforms to the zero wave energy boundary condition at land points used by ocean surface wave models and allows all the boundary cell faces to be treated in the same way as internal faces in one face loop. In addition, the periodic boundary condition for a global model is automatically included by the unstructured grid. So short boundary loops are avoided in the SMC grid propagation schemes and the full face and cell loops are streamlined for vectorization and parallelization.

An additional benefit of using two consecutive zero-boundary cells beyond the coastline is the complete blocking of wave energy by single-point islands. On a conventional lat-lon grid, wave energy can 'leak' through a single-point island due to the interpolation with neighbouring sea points in transport schemes which use a 5-point stencil like the UNO2 scheme. In the SMC grid, any single-point island is extended with two zero cells beyond its boundary face. As a result, wave energy cannot pass through such 'expanded island'. Nevertheless, sub-grid obstruction scheme from the original WAVEWATCH III model is kept to count for islands unresolved by the 6-km resolution. The sub-grid obstruction scheme follows the approach of Hardy et al (2000) with some modifications (Tolman 2003).

3.3. Refraction and spectral shift schemes

It should be emphasized that the linear surface wave theory is only valid when the water depth is non-zero (Falnes 2002). When h approaches zero, for instance, the refraction rate (2b) becomes undefined because the ξ factor approaches infinity (ξ ~ $0.5\sqrt{g/h}$). It is then customary in wave models to use a minimum water depth for the refraction term. A minimum water depth of 10 m is recommended and the refraction factor will then be less than 0.5.

Apart from shallow water depth, steep ocean floor and large time step may also result in a large refraction rate. For instance, if the discrete depth gradient is assumed to be $\Delta h/\Delta x = 0.1$ and time step is $\Delta t = 1000$ s, the maximum refraction angle per time step might be $\Delta t\Delta h/2\Delta x$ ~ 50 rad or about 8 full circles, which is no longer physically meaningful and is too large to fit into any advection-like refraction schemes used in contemporary wave models. One way to avoid this unrealistic large refraction increment is to use a small time step but this usually turns out to be too restrictive for wave models. Since refraction in a wave model is usually a minor process and is confined to coastal regions, the refraction increment is simply reduced to fit for the advection-like CFL condition in some wave models (WAMDI group 1988, Booij et al 1999, Tolman etal 2002). The CFL condition requires the refraction angle increment per time step to be less than one directional bin width (about 10º) and, of course, reduces the refraction effect. The latest version of the WAVEWATCH III model uses sub-time step to relax this restriction on the refraction term.

Here for the SMC grid wave model, a rotation scheme is substituted for the advection-like scheme to estimate the refraction term so that the CFL limit can be avoided. The rotation scheme is similar to a re-mapping advection scheme and is unconditionally stable. Although the rotation scheme does not have any limit on the refraction increment, the refraction angle should not pass beyond the depth gradient line (where $\mathbf{n}\cdot\nabla h = 0$) as stated in the refraction rate (2b). This physical limiter on the total refraction angle is included in the rotation scheme. The angle between the spectral direction and the depth decrease direction is calculated by:

$$\gamma = \cos^{-1}\left[-\left(h_x\cos\theta + h_y\sin\theta\right)\Big/\sqrt{h_x^2 + h_y^2}\,\right] \tag{9}$$

where h_x and h_y are the water depth gradient along x and y axis, respectively. Because FORTRAN function ACOS returns value between 0 and π, the maximum refraction angle (absolute value) is then chosen to be less than π/2 with $\Delta\theta_{mxrfr} = \min(\eta, \gamma, \pi - \gamma)$. The constant η (< π/2) is a user-defined maximum refraction angle to reduce the refraction effect if required. If η is set to be less than one directional bin width, the rotation scheme will be equivalent to the original advection-like scheme in the WAVEWATCH III model without using sub time steps. For the present comparison study, the refraction limiter is set to be π/3. This refraction limiter may prevent all directional components from converging at the depth gradient direction within one time step, which may result in unrealistic large wave energy like caustics in ray tracing models. It also creates room for merging the refraction with other directional changing terms, such as the refraction by ambient current and the GCT term.

The GCT term (3) can be fit into an advection-like scheme because it is usually less than one directional bin (~ 10º). For instance, if the time step is less than 900 s, the GCT angle (3) will be less than 1º per time step below 85º latitude, as the wave propagation angular speed, c_g/r, is on the order of 10^{-6} rad s^{-1}. However, as the refraction term is calculated with a rotation scheme in the SMC grid model, the GCT term is simply appended to the refraction term to form a total rotation angle. The rotation subroutine rotates each directional component by the combined angle and partitions its energy into the two directional bins which the rotated one strides across after the rotation. This simple rotation subroutine not only removes the time step restriction on the refraction angle but also adds an implicit diffusion in the θ direction because its implicit diffusivity is equivalent to that of the first order upstream scheme. This additional smoothing in the transverse direction is desirable for wave models to mitigate the GSE.

The spectral shift term, fourth in (1), is calculated with an advection-like UNO2 scheme in the k-space because the spectral shift is usually small enough to meet the CFL condition. The term is calculated at the base time step for all cell spectra.

3.4. The polar problem

The ocean surface wave energy spectrum is usually defined as discrete directional components from a reference direction at the local east and each directional component is assumed to be a scalar in wave propagation. This scalar assumption has been taken for granted in finite difference schemes, such as, calculation of the local gradient, $G_{DC} = (\psi_D - \psi_C)/(x_D - x_C)$, where the vector components ψ_D and ψ_C for the two neighbouring cells are assumed to be at the same direction, that is, to be treated as a scalar. This scalar assumption is a good approximation for a global wave model when the ice covered Arctic area is excluded. However, the scalar assumption becomes erroneous at high latitudes on a reduced grid since the change of direction over one grid-length grows too large to be ignored. For instance, in the SMC6-25 grid (see Fig.1) there are 8 cells immediately around the polar cell, the local east direction changes by 45º over one cell length. The invalid scalar assumption based on local east reference direction in the polar region prevents extension of ocean surface wave models at high latitudes. This problem can be avoided by switching to a fixed reference direction, for instance, the map-east direction as viewed on a stereographic projection of the polar region. Assuming the angle from the map-east to the local east is α, the wave spectral component for a given direction of angle θ from the local east will have an angle $\theta' = \theta + \alpha$ from the map-east. Its zonal and meridian group speed components are then given by

$$\begin{aligned} c_g \cos\theta &= c_g \cos(\theta' - \alpha) \\ c_g \sin\theta &= c_g \sin(\theta' - \alpha) \end{aligned} \tag{10}$$

Note that the polar cell does not have a local east direction so the velocity could not be defined at the Pole as zonal and meridian components. In the SMC grid, however, only the meridian velocity component at the edge of the polar cell is required and there is no need to define the velocity at the polar cell centre. This is one of the advantages of using a polar cell centred at the Pole. Nevertheless, velocity components at the Pole can be defined in the fixed reference system but they could not be converted into the local east system.

Because a given direction θ' from the map-east is constant in the Arctic region, the spectral component in the map-east system can be treated as a scalar for transport in the polar region. For the velocity in a dynamical model, its components along the map-east ($\theta' = 0$) and map-north ($\theta' = \pi/2$) can also be approximated as a scalar in the polar region. Their transport velocity components in the standard grid are then given by (9) after substituting their corresponding component values (u' and v') for c_g, respectively. The polar cell can hold velocity or wave spectrum in the map-east system as scalars for transport but they do not need to be converted into the local east system.

This map-east direction can be conveniently approximated with a rotated grid with its rotated pole on the Equator. The standard polar region becomes part of the 'tropic region' in the rotated grid so the longitudinal direction of the rotated grid can be substituted for the map-east direction. For instance, if the rotated pole is at 180ºE on the Equator, the angle α from this map-east to the local east at longitude λ and latitude φ within the Arctic region can be worked out with:

$$\alpha = \mathrm{sgn}(\cos\varphi \sin\lambda) \arccos\left[\frac{\cos\lambda \sin\varphi}{\sqrt{1-(\cos\lambda\cos\varphi)^2}}\right] \tag{11}$$

If the map-east is used within the Arctic region and local east in the rest for definition of the wave spectrum, there will be no fixed corresponding components between the two systems because α varies with longitude and latitude. For this reason, wave spectra defined by local east could not be mixed up with those defined from the map-east and the Arctic region using the map-east reference direction has to be separated from the rest which uses local east reference directions. In the SMC grid shown in Fig.1, the reference direction change is set between the 3rd (at about 83º) and 4th (at 86.4º) size-changing parallels (see definition in Li 2011), where the local east direction changes less than 3º over one cell length as there are 128 cells in one row. The Arctic part and the rest (will be referred to as the *global part*) are linked together through 4 over-lapping rows. Wave spectra in the lower two of the 4 over-lapping rows in the Arctic part are updated with wave spectra from the global part after they are rotated anticlockwise by α. Wave spectra in the upper two rows of the 4 over-lapping rows in the global part are updated with wave spectra from the Arctic part after a clockwise rotation by α. Because of the unstructured nature of the SMC grid, the Arctic cells are appended behind the global part in the single cell list for propagation. The two parts can be conveniently separated by using sub-loops. The overlapping rows are treated in the same way as other cells so the propagation is calculated together for both parts. Wind direction and other direction related source terms have to be modified within the Arctic part to use the map-east reference direction.

If only the velocity components are dealt with within the Arctic (such as in a dynamic model), there is no need to work out the angle itself. The cosine and sine of the rotation angle will be enough for velocity conversion between the map-east and local east system. The rotation angle cosine and sine are given by

$$\cos\alpha = \frac{\cos\lambda \sin\varphi}{\sqrt{1-(\cos\lambda\cos\varphi)^2}}, \qquad \sin\alpha = \frac{\sin\lambda}{\sqrt{1-(\cos\lambda\cos\varphi)^2}}, \tag{12}$$

The conversion between the map-east velocity components *u'* and *υ'* and the local east velocity components *u* and *υ* are given by

$$\begin{pmatrix} u' \\ \upsilon' \end{pmatrix} = \begin{pmatrix} \cos\alpha & -\sin\alpha \\ \sin\alpha & \cos\alpha \end{pmatrix} \begin{pmatrix} u \\ \upsilon \end{pmatrix}, \qquad \begin{pmatrix} u \\ \upsilon \end{pmatrix} = \begin{pmatrix} \cos\alpha & \sin\alpha \\ -\sin\alpha & \cos\alpha \end{pmatrix} \begin{pmatrix} u' \\ \upsilon' \end{pmatrix} \tag{13}$$

That is, the local east velocity vector is rotated anticlockwise by the angle α as viewed in the map-east system. The wind component relationship (12) may also be used in the Arctic part to convert the local east wind to the map-east wind for wave model source terms.

4. Comparison with global and regional models

A global SMC grid model similar to the SMC6125 model here but without the refinement of 12 km resolution in the European region (SMC6-25) has been compared with a regular grid global model at 25km resolution (G25), the same base resolution of the SMC6125 model. It has been shown that the SMC6-25 model is comparable with the G25 model and the results are available in Li (2012). A comparison of the SMC6125 model with the previous SMC6-25 model has confirmed that the

SMC6125 model performs very similarly to the SMC6-25 model and has better performance in the European region than the SMC6-25 model because of the increased resolution. An Arctic view of the SWH field from the SMC6125 model is shown in Fig.3 and it confirms that the minimum sea ice edge around the beginning of September 2012 is still below 86ºN, within the global part of the SMC6125 model. So the Arctic part of the SMC6125 model (above the yellow circle in Fig.1 or Fig.3) has not been activated for this study. Comparison of the SMC6125 model with 30 spectral buoys for four months, September-December 2012, is shown in Fig.4, which shows both the SWH and 4 sub-range wave height (SRWH) scatter plot (details see Li and Saulter 2012) and is comparable with that of the SMC6-25 model as shown in Fig.5 of Li (2012).

Here the comparison will be concentrated on our operational models, including the global 30 km multi-grid model (G30), the European 8 km model (Euro8) and the 4 km model around the UK waters (UK4). The G30 model uses a multi-grid version of the WW3 model with the middle main domain covering from 65.5°S to 72.0ºN at a resolution of about 30 km and two polar stripes connecting the main domain to the polar regions at reduced resolution of about 60 km. It is not a surprise that the SMC6125 model is better than the G30 model because the SMC6125 model resolution is, overall, better than the G30.

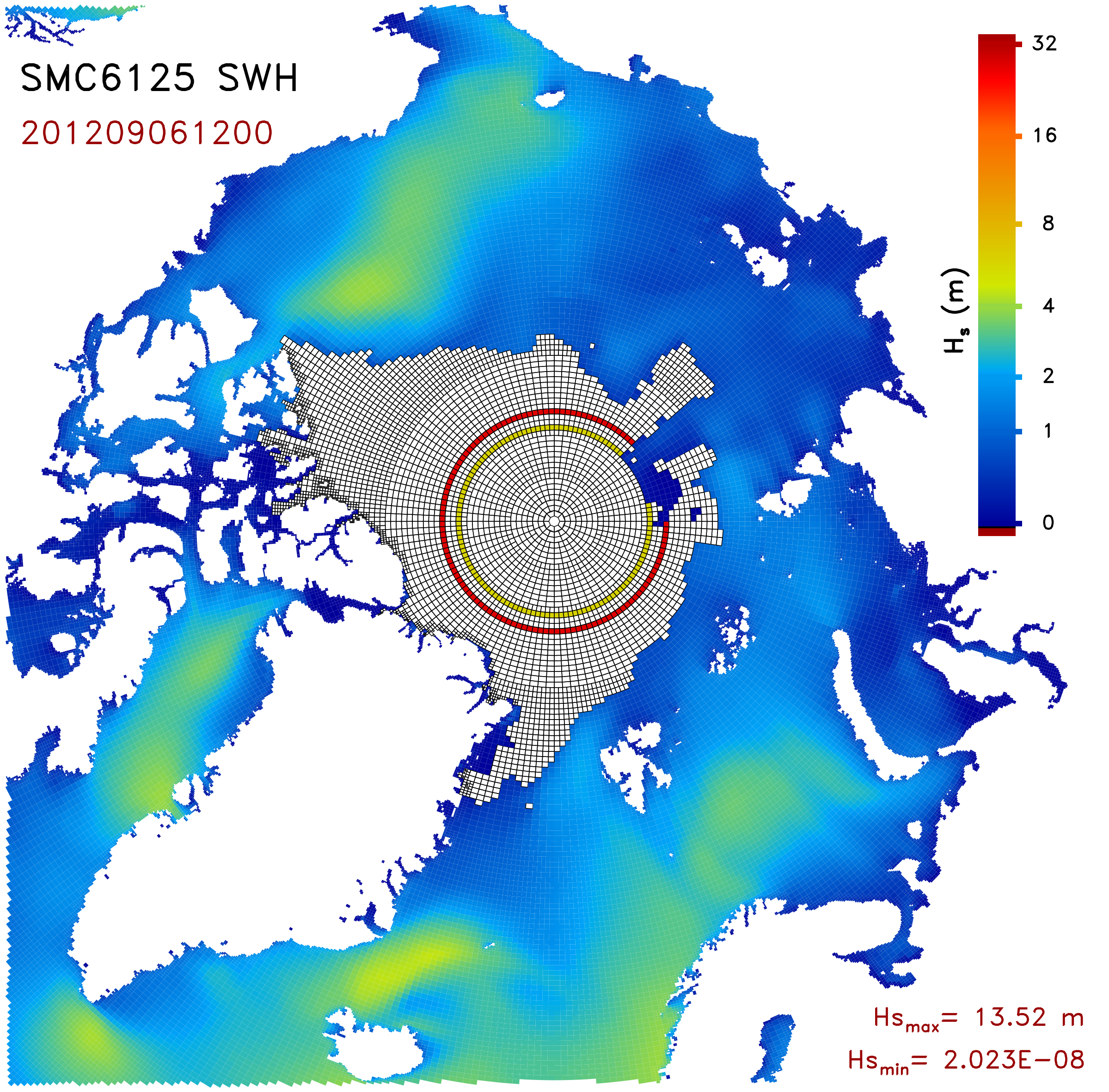

Fig.3. SWH from SMC6125 model at 1200 hr on 06 September 2012, close to the minimum Arctic sea ice in summer 2012.

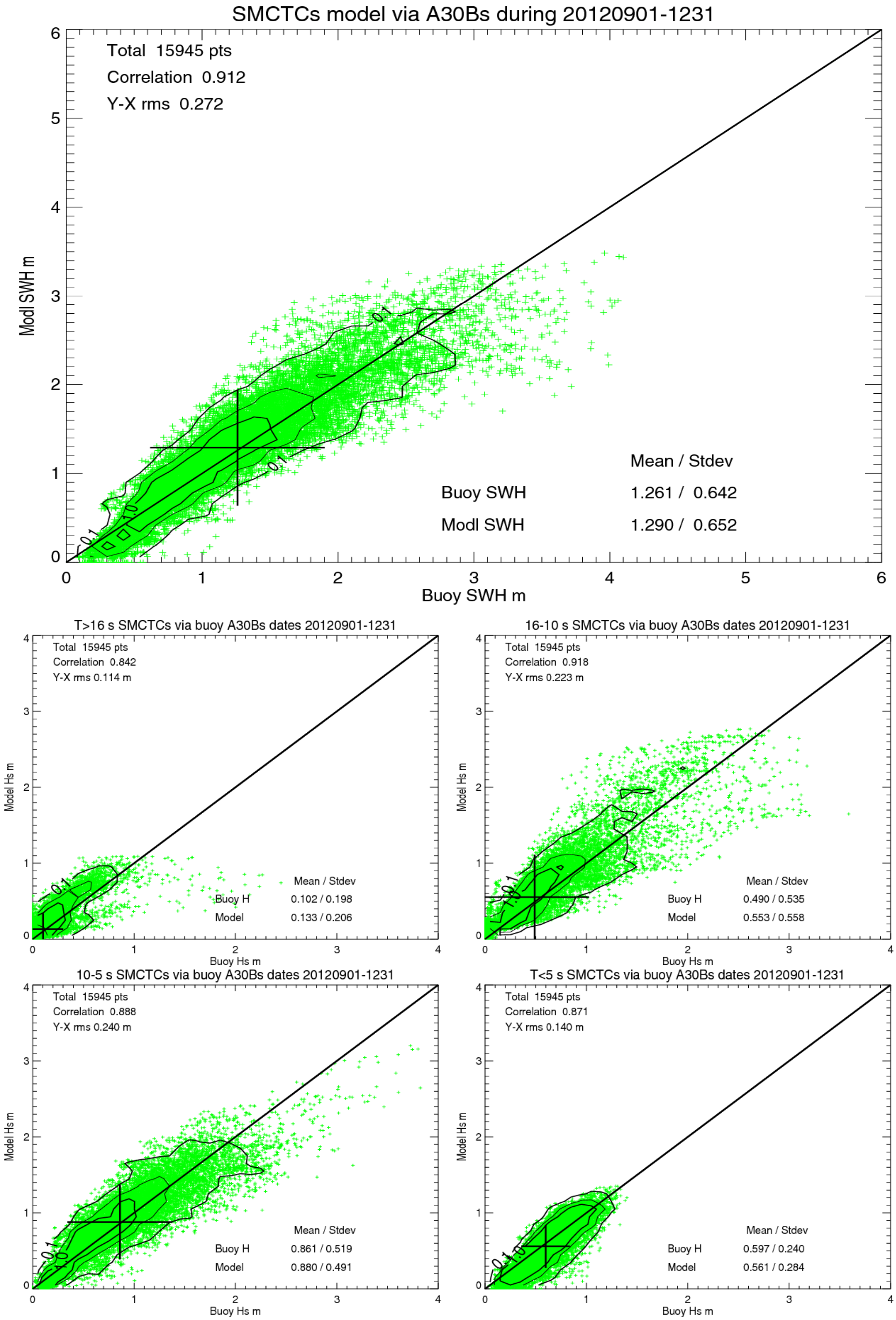

Fig.4. Comparison of SMC6125 model SWH with 30 spectral buoys form 1 September to 31 December 2012 (top single panel) and their 4-bin SRWH break down (bottom 4-panels).

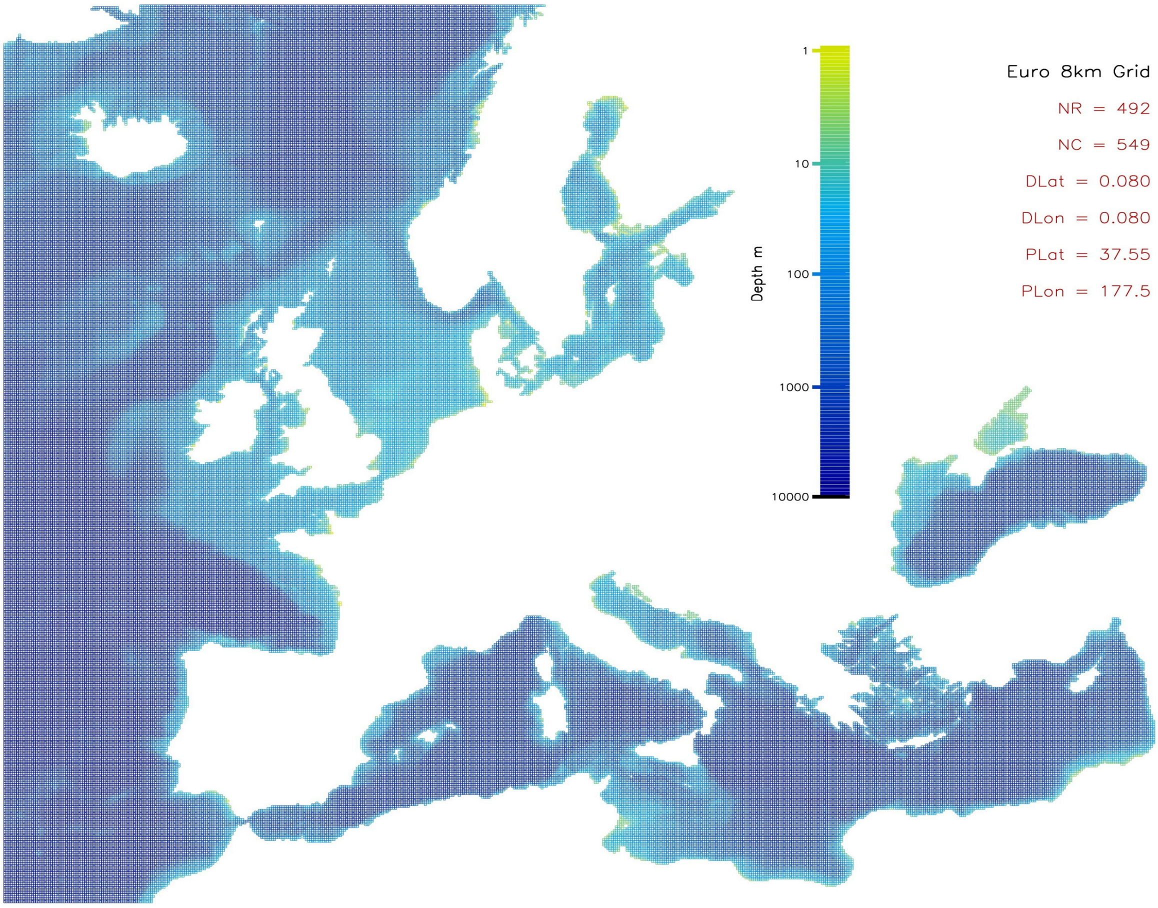

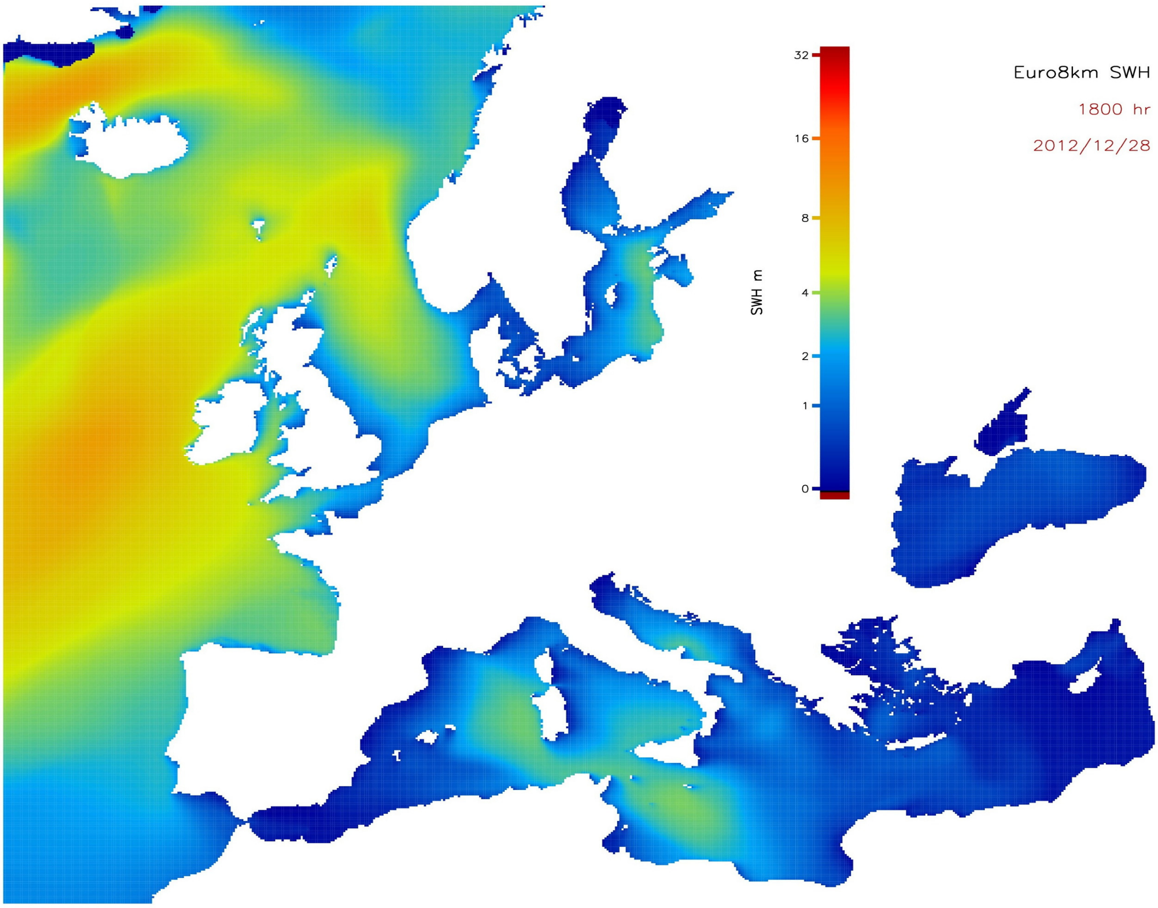

Fig. 5. Met Office European 8 km operational wave model grid and swh on 20121228 at 18 hr.

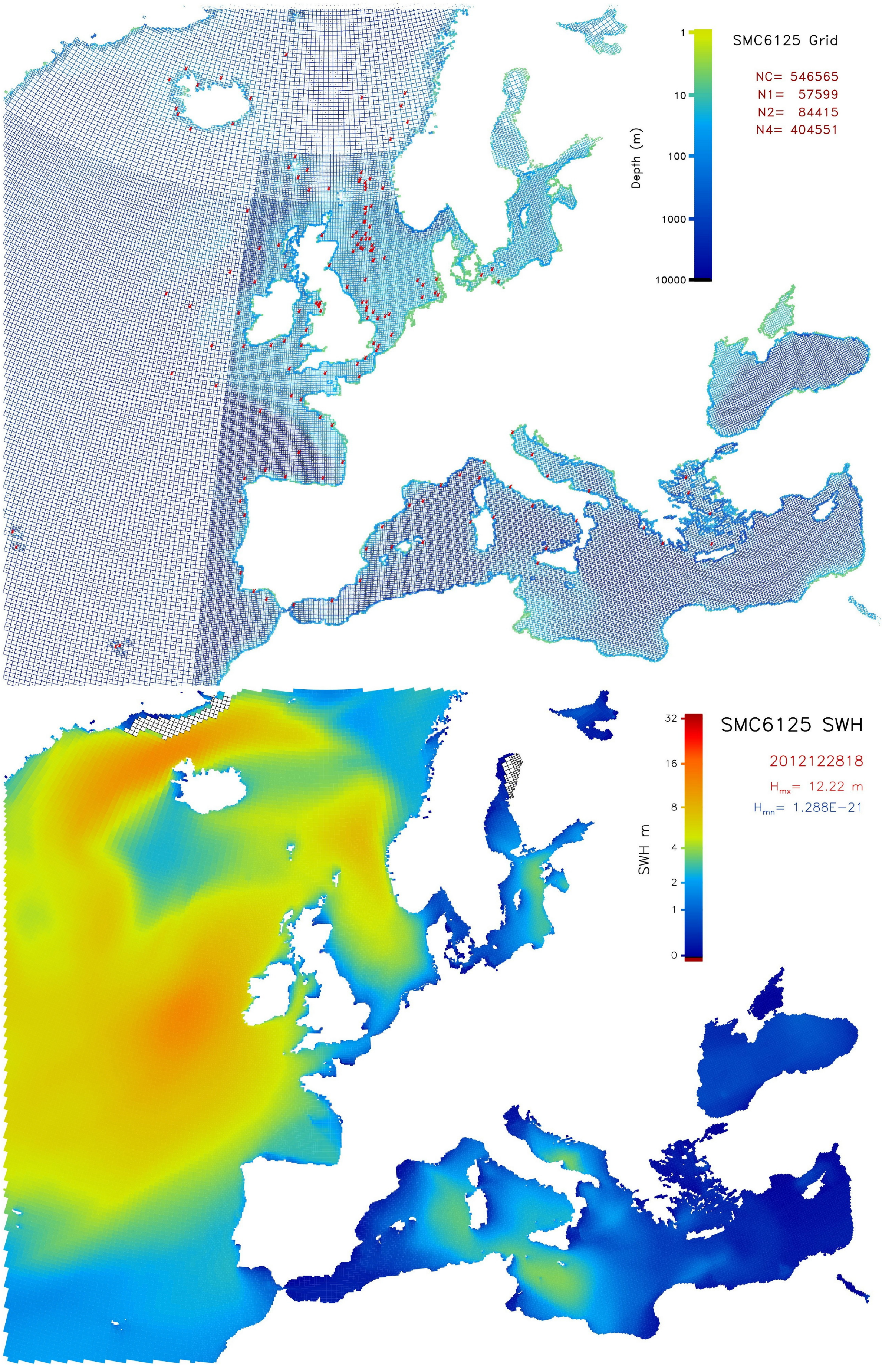

Fig. 6. SMC6125 model grid and swh around the Euro 8km model area for comparison.

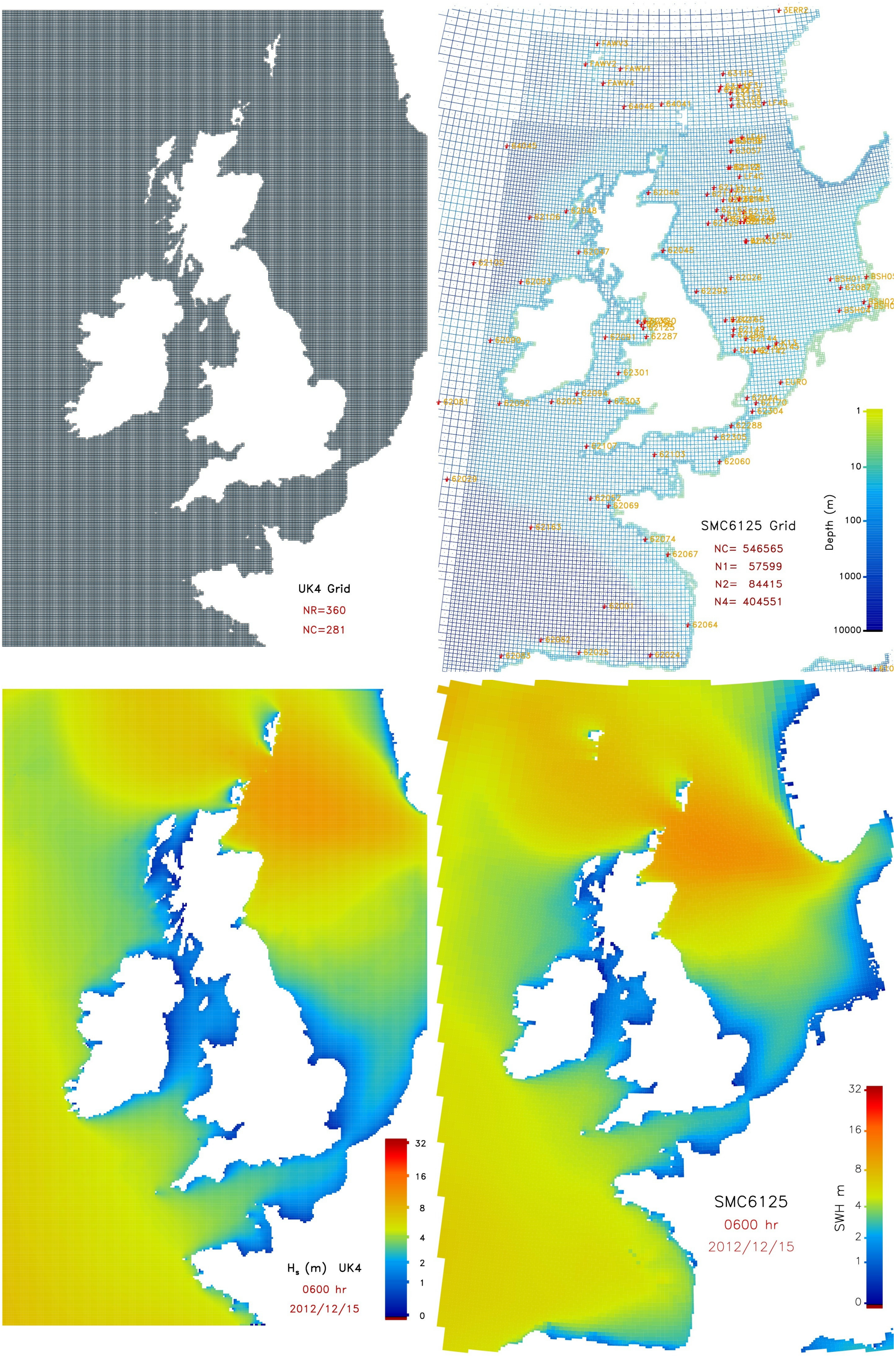

Fig.7. Comparison of UK4 and SMC6125 grids and SWH on 15 Dec 2012.

The Euro8 model is framed on a rotated grid, covering roughly 25ºW to 45ºE and 30ºN to 70ºN at constant resolution of 0.08º at both directions. Fig.5 shows the Euro8 model grid and its typical SWH output on 28 December 2012. The rotated N-Pole is at 177.5ºE and 37.55Nº so the rotated Equator is about 52ºN at zero meridian, or approximately crossing London, UK. Fig.6 shows the corresponding model grid and SWH plots from the SMC6125 model around the area covered by the Euro8 model. Because the SMC6125 grid uses standard lat-lon meshes, its size-2 longitudinal resolution in the refined European region has shrunk close to that of the Euro8 model due to increased latitudes. The small '+' symbols in the SMC6125 grid plot indicate the positions of ocean wave buoys used for this model comparison.

The UK4 model is also on the same rotated grid as the Euro8 model but at the higher resolution of 0.04º for both lat and lon dimensions. Its grid and SWH plots are shown in Fig.7 along side with the corresponding ones from the SMC6125 model. The size-1 cell is very close to the UK4 cell while the size-2 cells are more than doubled the UK4 cells. So the SMC6125 grid is coarser than the UK4 except for near the coastlines.

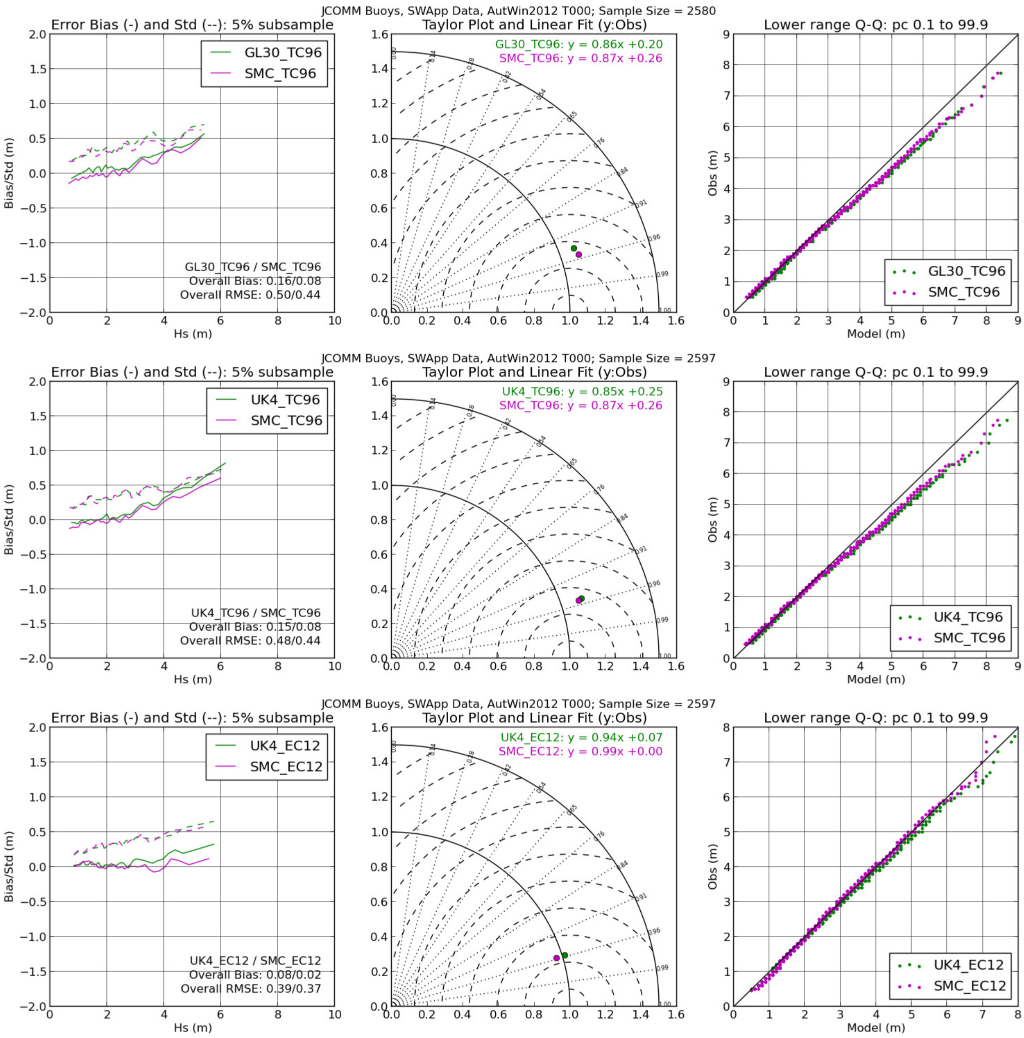

Fig.8. Comparison of performance of Global (30km), SMC6125 and UK4 (4km, nested within Global) wave models in prediction of significant wave height for in-situ platforms in the Southwest Approaches to the UK. Plots in columns from left to right show bias and RMSE through 5% subsamples of the model significant wave height range; Taylor plot; and Quantile-Quantile plot of data at 0.1% intervals from 0.1-99.9%.

Fig.8 and Fig.9 show results of a verification comparison between the SMC6125 and test configurations of the operational G30 and UK4 wave models. The verifying data in these cases were taken from in-situ platforms contributing to the JCOMM inter-comparison of operational ocean wave forecasting systems (Bidlot et al., 2002). The two examples illustrate the performance of the SMC model in environments where the proximity of land will affect the fetch to the measurement locations in a number of directional sectors. In the Southwest Approaches case (Fig.8) the influence of waves generated in open waters of the Atlantic is expected to be more significant than in the case of the Central North Sea (Fig.9).

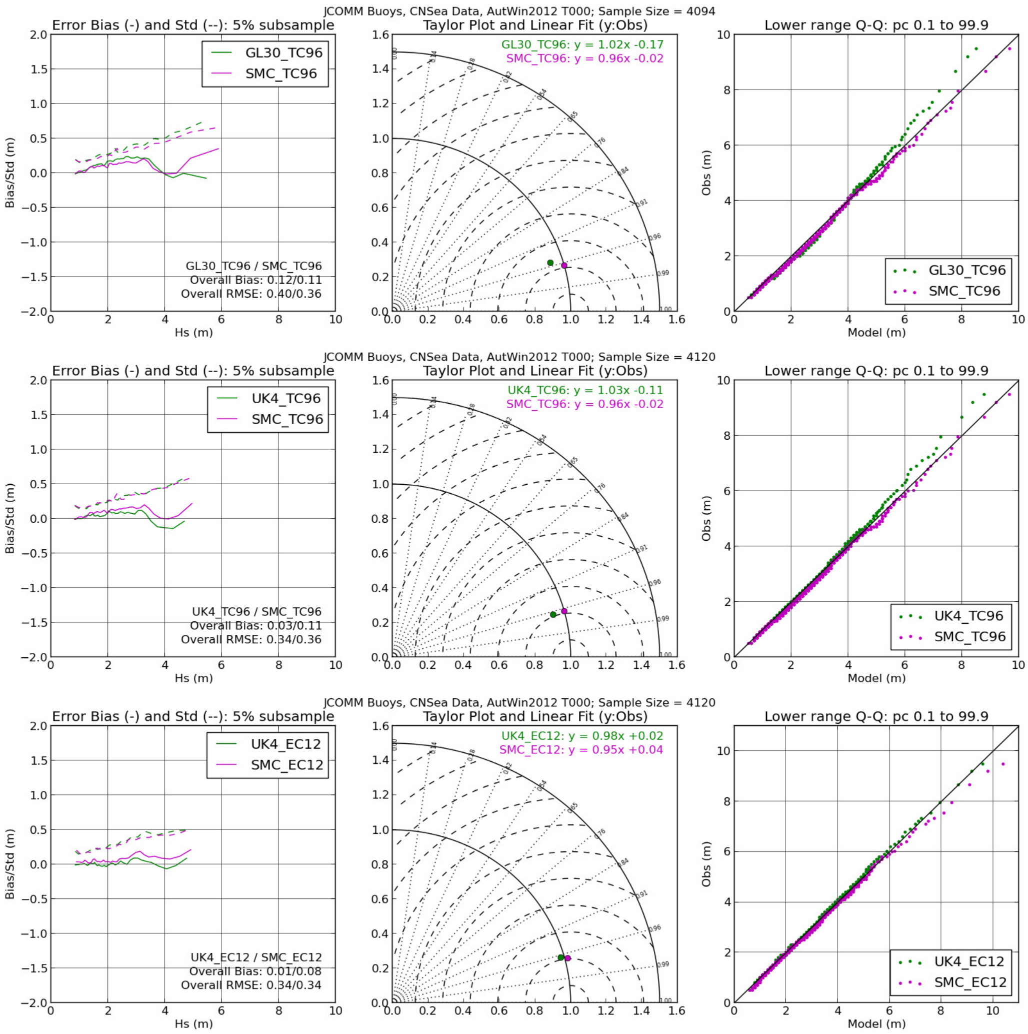

Fig.9. Same as Fig.8 but for in-situ platforms in the Central North Sea.

The upper row of panels in Fig.8 compare the G30 and SMC6125 models when run using Tolman and Chalikov (1996, TC96) source terms. Although both models show a trend for over-prediction at significant wave heights over 4m (upper left and right panels), a substantive improvement in bias, RMSE and correlation (shown by a shift toward the x-axis in the Taylor plot) can be seen for the SMC6125 data. The central row of panels shows a comparison between SMC6125 and UK4 models using the TC96 physics. Although correlation is improved in the UK4 configuration compared to the G30 data (upper-centre and centre-centre panels), the influence of the G30 boundary conditions are such that the overall bias and RMSE performance of the SMC6125 configuration is still better than the UK4. In the lower row of panels versions of the SMC6125 and UK4 models using WAM4 derivative physics following Bidlot (2012, EC12) are compared. The use of the revised physics package significantly improves performance of both models, particularly in terms of bias for wave heights beyond 4m (right hand panels) and relative standard deviation of the model versus observed data (centre panels). The comparison between the two models is closer, but still puts the SMC6125 ahead of the UK4, probably because the UK4 in this run was still nested into a TC96 version of the G30.

In the Central North Sea case (Fig.9) the panels are set out using the same runs as described previously. Again a substantive improvement can be seen between SMC6125 and G30 models in terms of RMSE, correlation and (this time) prediction of significant wave heights above 4m. With the influence of the global boundary condition weakened in this region, performance of the UK4 and SMC6125 TC96 driven models (central panels) is similar. Application of the EC12 source terms leads to improvement of the UK4 prediction of high sea states (lower right panel) and improvement in correlation for the SMC6125 model (lower centre panel). The two models are shown to compare very closely in this instance.

Comparison of in-situ platform observations with the Euro8 model yields similar result as the SMC6125 model but the result is not shown here. Overall these examples suggest that the SMC model is capable of meeting its designated aims, i.e. to provide an improvement beyond a regular grid global model and achieve similar levels of accuracy to a high resolution nested model in regional seas. Although subject to further testing these results appear to be robust to changes in the source term physics used by the model.

5. Other example of SMC grids

i) Atlantic SMC6-25 grid

The Atlantic SMC6-25 grid shown in Fig.10 is a regional selection of the global SMC6-25 cells over the Atlantic Ocean. Thanks to its unstructured nature of the SMC grid, a portion of the global cells can be regrouped to form a regional model. To minimise boundary input, the selected Atlantic domain follows coastlines all the way from the Antarctic to Arctic except for a few short cross-sections, particularly the two over the Sothern Ocean, between the Cape Horn in S America (69W) and Cape Agulhas (20E) at the tip of S Africa. The Atlantic domain is retuned to remove unimportant branches at the outskirts, such as the Gulf of Mexico, the Hudson Bay, and the Mediterranean.

Only the two cross-sections in the Southern Ocean are fed with boundary conditions for the Atlantic model. Boundary conditions at Strait of Gibraltar, Baltic Sea, Gulf of Mexico (La Habana - Miami), Hudson Bay, and Baffin Bay are ignored as they are either quite small or sheltered by nearby islands. In WW3, boundary conditions are applied by defined grid points which can be anywhere in the grid. As SMC grid works with boundary points in the same way as in the regular grid, there is no major issue in adding boundary data except for definition of the boundary cells. The boundary data for the Atlantic model can be generated either by a regular grid or the SMC grid global model.

The Atlantic SMC6-25 grid is presently used in the Met Office ensemble forecast. Fig.11 shows a SWH 'postage stamps' at T+54 for the North Atlantic from a 24 member wave ensemble presently under evaluation at the Met Office. Ensemble perturbations are introduced by variations in the forcing winds and (member consistent) starting conditions using the T+6 forecast condition from the previous run. The members show considerable differences in development of very rough or higher seas between Greenland and the UK, and in the development of waves under Tropical Storm Humberto.

ii) The Great Lakes SMC0512 grid

Fig.13 is a regional model to cover the Great Lakes at variable resolution from 0.5km to 2 km. As the Great Lakes are isolated from the oceans, this model domain does not need any boundary conditions. Also note the southern edge of the corresponding regular grid at 2km resolution is above the Equator so the SMC grid reference origin for the y-indices is no longer on the Equator but at the southern edge of the regular grid. The bathymetry data are from NCEP/NOAA and the water depth has been adjusted to be relative to the low water level in each lake. A test run forced with the Met Office 25km global wind for one month in Sept 2012 (with 10 days spinning up) has show that the model matches well with surface wave observations from the spectral buoys marked in Fig.13. A SWH field with the maximum SWH during this one month run is shown in Fig.14. The wind sea is slightly underestimated due to the coarse wind forcing and there is hardly any swell in the Great Lakes due to the limited fetch. These spectral features are illustrated with the 4-bin SRWH scatter plot shown in Fig.12. The long swell bin (T>16 s) is almost empty and most wave energy is concentrated in the short wave bins (T< 5s and 5-10 s).

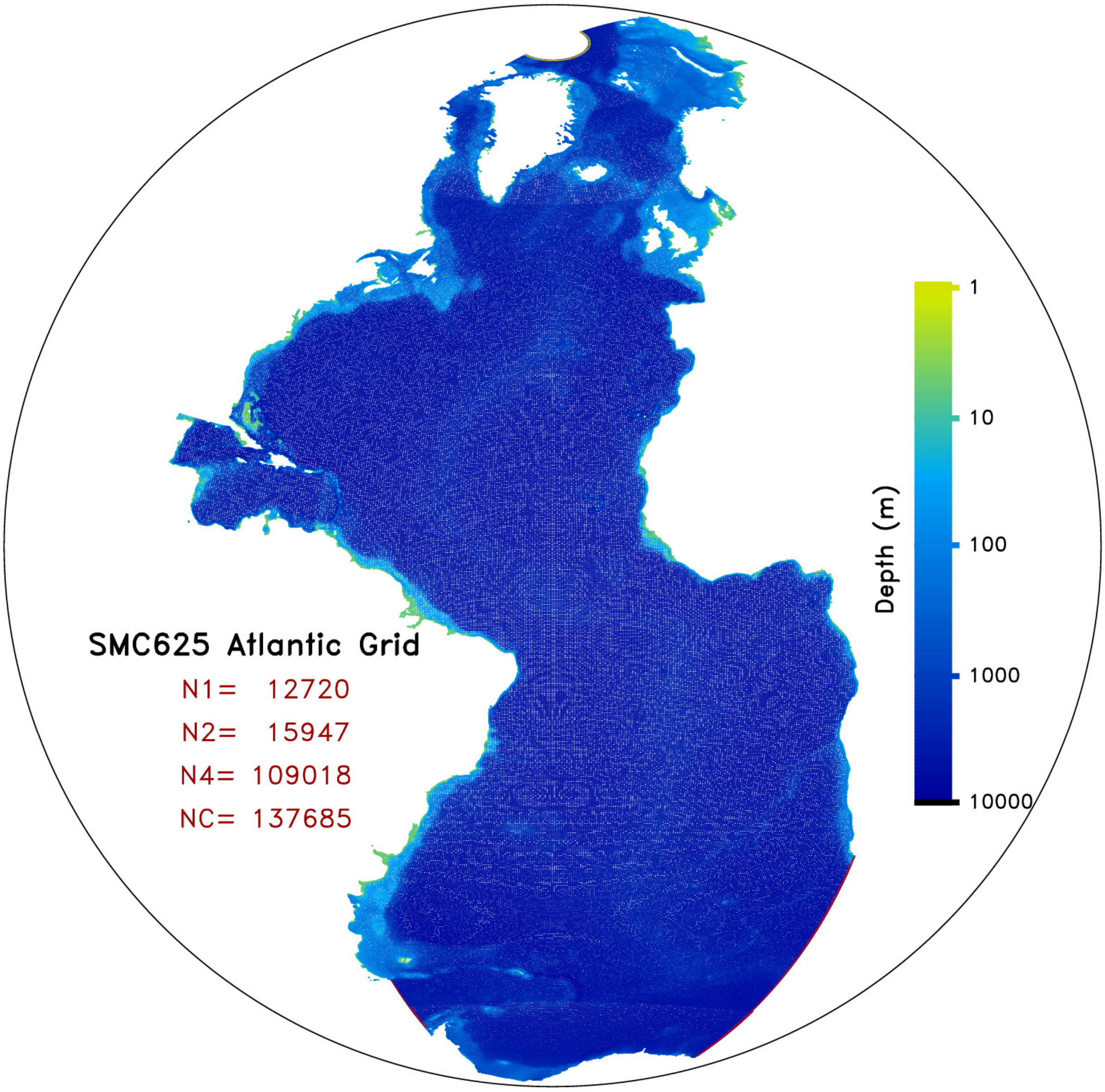

Fig. 10. The Atlantic SMC6-25 grid for ocean surface wave model.

6. Conclusions

Results indicate that the SMC6125 is better than the G30 global model and comparable with the two regional models at higher resolutions. The SMC6125 model cpu time is slightly longer than the G25 one, due to increase of cell numbers at refined resolutions and the requirement to use an irregular grid UNO2 advection scheme. Improvement may be possible if regional high resolution wind forcing could be blended with the global wind field and used to drive the high resolution part of the SMC6125 model, as in these experiments the whole domain was driven by 25km wind forcing. Nevertheless, the unified wave model is capable of replacing the present global and nested regional operational suite, greatly simplifying the operational wave forecasting job without sacrifice of accuracy. Applications of the SMC grid for regional models will also benefit from the unstructured feature and variable resolutions.

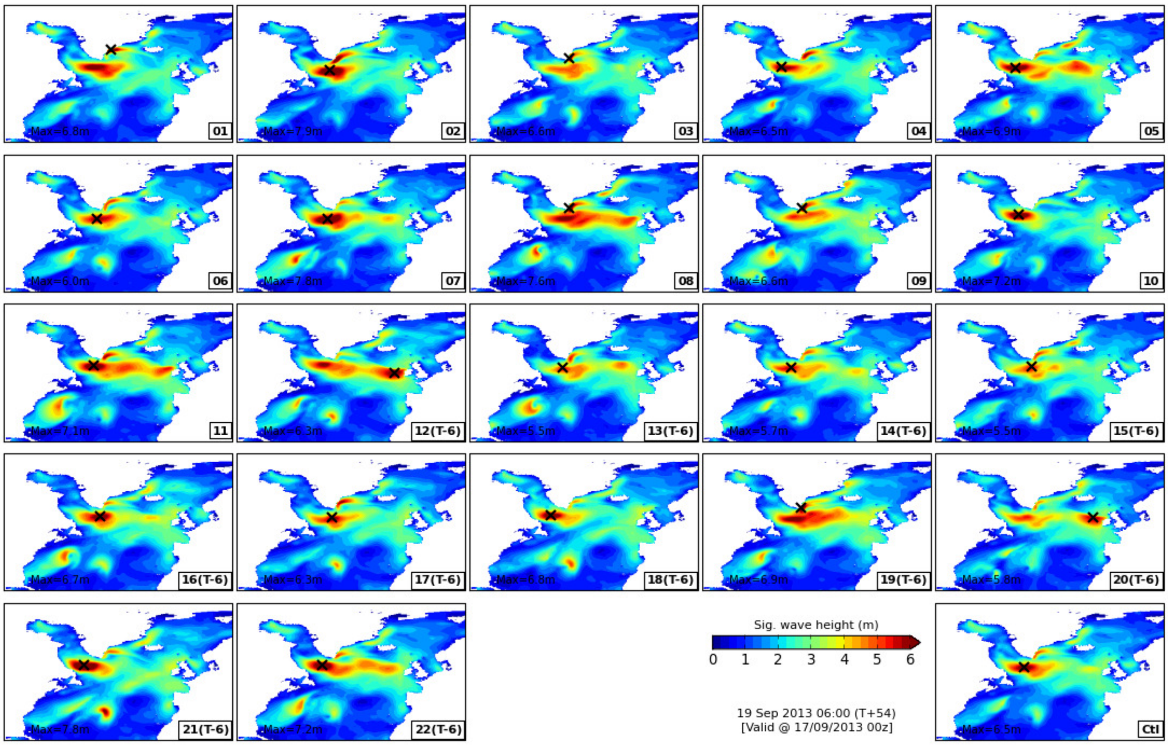

Fig.11. Ensemble forecast of SWH from the Atlantic SMC6-25 model.

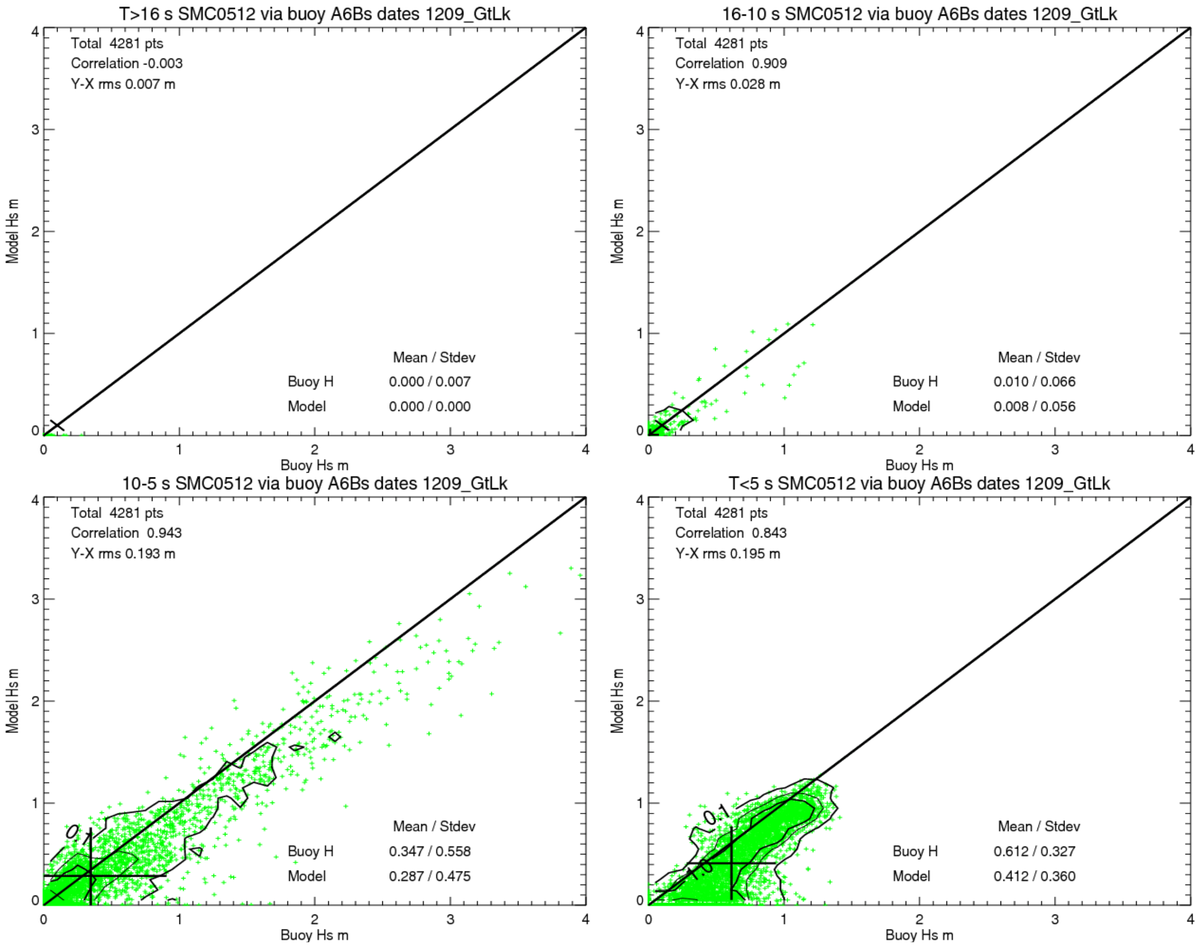

Fig.12. Four-bin SRWH comparison with spectral buoys for the Great Lakes over September 2012.

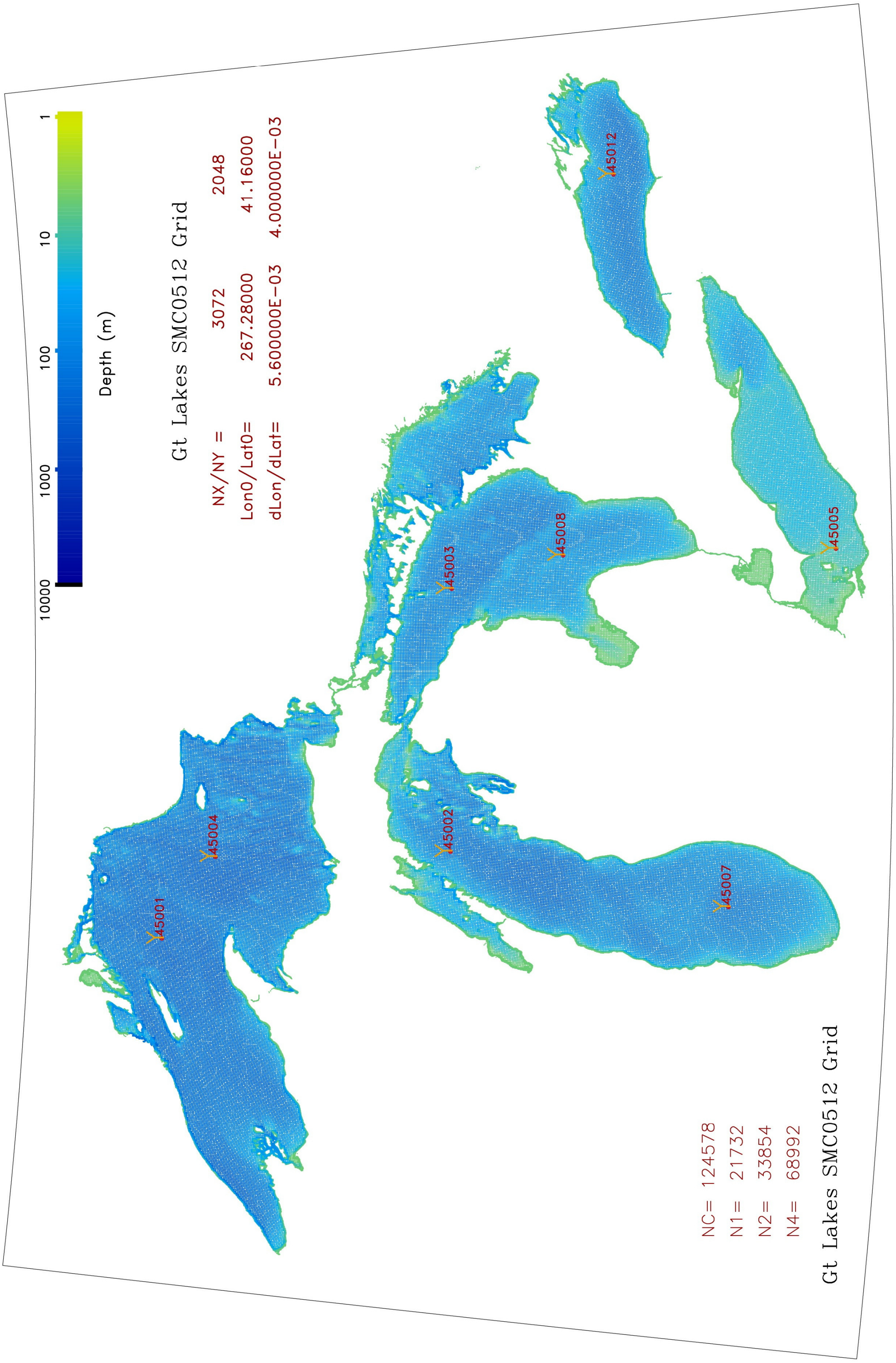

Fig.13. The SMC0512 grid for the Great Lakes.

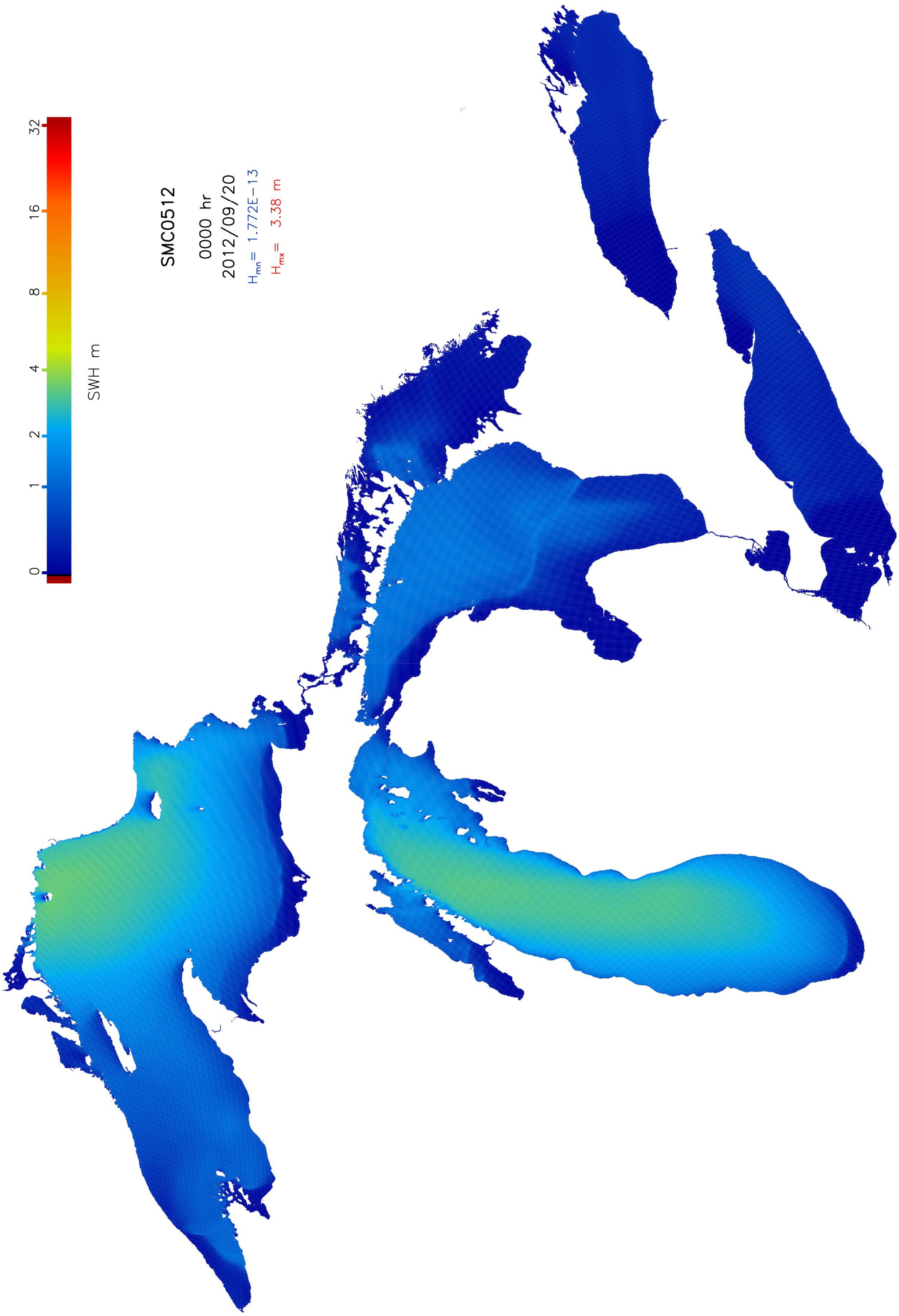

Fig.14. Simulated SWH field from SMC0512 model for the Great Lakes on 20 September 2012.

References

Bidlot, J.R., 2012: Present status of wave forecasting at ECMWF. *Proc. ECMWF Workshop on Ocean Waves*, 25-27 June 2012, ECMWF, Reading, UK. p1-15.

Bidlot, J.R., D.J. Holmes, P.A. Wittmann, R. Lalbeharry, and H.S. Chen, 2002: Intercomparison of the performance of operational ocean wave forecasting systems with buoy data. *Weather and Forecasting*, **17**, 287-310.

Booij, N., and L.H. Holthuijsen, 1987: Propagation of ocean waves in discrete spectral wave models. *J. Comput.* Phys., **68**, 307-326.

Booij, N., R.C. Ris, and L.H. Holthuijsen, 1999: A third-generation wave model for coastal regions, 1. Model description and validation. *J. Geophys. Res*. **104,** C4, 7649-7666.

Chawla, A., and H.L. Tolman, 2008: Obstruction grids for spectral wave models. *Ocean Modelling,* **22**, 12-25.

Falnes, J., 2002: *Ocean Waves and Oscillating Systems*. Cambridge University Press, Cambridge, UK, 275 pp.

Hardy, T.A., L.B. Mason, and J.D. McConochie, 2000: A wave model for the Great Barrier Reef. *Ocean Engineering*, **28**, 45-70.

Li, J.G., 2008: Upstream non-oscillatory advection schemes. *Mon. Wea. Rev*., **136**, 4709-4729.

Li, J.G., 2011: Global transport on a spherical multiple-cell grid. *Mon. Wea. Rev*., **139**, 1536-1555.

Li, J.G., 2012: Propagation of Ocean Surface Waves on a Spherical Multiple-Cell Grid. *J. Comput. Phys*., **231,** 8262-8277.

Li, J.G. and A. Saulter, 2012: Assessment of the updated Envisat ASAR ocean surface wave spectra with buoy and altimeter data. *Remote Sensing of Environment*, **126**, 72-83.

Phillips, O.M., 1977: *The Dynamics of the Upper Ocean*. 2nd Ed., Cambridge Univ. Press, Cambridge, UK, 336 pp.

Rasch, P.J., 1994: Conservative shape-preserving two-dimensional transport on a spherical reduced grid. *Mon. Wea. Rev*., **122**, 1337-1350.

Roe, P.L., 1985: Large scale computations in fluid mechanics. in: E. Engquist, S. Osher, R.J.C. Sommerville (Eds.), *Lectures in Applied Mathematics*, **22**, 163-193.

Roland, A., A. Cucco, C. Ferrarin, T.-W. Hsu, J.-M. Liau, S.-H. Ou, G. Umgiesser, and U. Zanke, 2009: On the development and verification of a 2-D coupled wave-current model on unstructured meshes. *J. Marine Sys*., **78** SUPP, S244-S254.

Tolman, H.L., 1991: A third-generation model for wind waves on slowly varying unsteady and inhomogeneous depths and currents. *J. Phys. Oceanogr*., **21**, 782-792.

Tolman, H.L., 2002: Alleviating the Garden Sprinkler Effect in wind wave models. *Ocean Modelling*, **4**, 269-289.

Tolman, H.L., 2003: Treatment of unresolved islands and ice in wind wave models. *Ocean Modelling*, **5**, 219-231.

Tolman, H.L., 2008: A mosaic approach to wind wave modeling. *Ocean Modelling*, **25**, 35-47.

Tolman, H.L., B. Balasubramaniyan, L.D. Burroughs, D.V. Chalikov, Y.Y. Chao, H.S. Chen, and V.M. Gerald, 2002: Development and implementation of wind-generated ocean surface wave models at NCEP. *Weather and Forecasting,* **17,** 311-333.

Tolman, H.L. and D. Chalikov, 1996: Source terms in a third-generation wind-wave model. *J. Phys. Oceanogr.*, **26**, 2497-2518.

WAMDI group, 1988: The WAM model - a third generation ocean wave prediction model. *J. Phys. Oceanogr*., **18**, 1775-1810.

WISE Group, L. Cavaleri, J.-H.G.M. Alves, F. Ardhuin, A. Babanin, M. Banner, K. Belibassakis, M. Benoit, M Donelan, J. Groeneweg, T.H.C. Herbers, P. Hwang, P.A.E.M. Janssen, T. Janssen, I.V. Lavrenov, R. Magne, J. Monbaliu, M. Onorato, V. Polnikov, D. Resio, W.E. Rogers, A. Sheremet, J. McKee Smith, H.L. Tolman, G. van Vledder, J. Wolf, and I. Young, 2007: Wave modelling - the state of the art. *Progress Oceanogr.,* **75,** 603-674.